Greul E, Petrus ML, Binek A, Docampo P, Bein T.

Highly stable, phase pure Cs2AgBiBr6 double perovskite thin films for optoelectronic applications.

***Journal of Materials Chemistry A* 2017, 5(37), 19972-19981.**

Journal Name

ARTICLE

Highly stable, phase pure $Cs_2AgBiBr_6$ double perovskite thin films for optoelectronic applications

Received 00th January 20xx,
Accepted 00th January 20xx

DOI: 10.1039/x0xx00000x

www.rsc.org/

Enrico Greul,[a] Michiel L. Petrus,[a] Andreas Binek[a], Pablo Docampo[b] and Thomas Bein[a]*

Hybrid lead halide perovskites have emerged as high-performing semiconductors for optoelectronic applications such as photovoltaics. However, their toxicity and stability issues represent significant challenges. Recently, double perovskites have been suggested as an alternative and, especially, Cs_2AgBiX_6 (X = Cl, Br) has proved to be a promising material as it is non-toxic and highly stable. However, the low solubility of precursors has so far hampered the fabrication of high quality films. Here, we demonstrate for the first time the fabrication of $Cs_2AgBiBr_6$ films and incorporate them into working devices. Powder X-ray diffraction measurements revealed that high annealing temperatures of at least 250 °C are required to fully convert the precursors into $Cs_2AgBiBr_6$. After the optimization of the synthesis conditions, photovoltaic devices comprising our $Cs_2AgBiBr_6$ films show power conversion efficiencies (PCE) close to 2.5% and a open circuit voltage (V_{oc}) exceeding one volt, which is currently the highest V_{oc} reported for a bismuth halide based perovskite, showing the potential of double perovskites as the absorber material. Furthermore, our results revealed excellent stability of the devices upon exposure to working conditions without encapsulation. Our work opens the way to a new class of perovskites with significant potential for optoelectronic applications.

Introduction

Since the first reports of solid-state solar cells in 2012, hybrid organic-inorganic lead halide perovskites emerged as some of the most promising absorber materials for low-cost photovoltaic devices.[1] Published PCEs of over 22% make these materials potential candidates for replacing commonly employed Si-based solar cells.[2] Despite their excellent photophysical properties,[3–8] lead halide perovskites still suffer two serious disadvantages, namely stability issues and the toxicity of lead.[9–12] Many research groups have therefore focused on the development of more stable and/or lead-free perovskite materials. Substitution of the Pb^{2+} by the homovalent group-14 element Sn^{2+} initially led to promising PCEs of ~ 6%. However, the devices showed extremely low stability, even under commonly used inert conditions, due to the facile oxidation of Sn^{2+}. So far, this makes Sn^{2+}-based materials unfeasible for typical photovoltaic applications.[13,14] A recent approach towards lead-free perovskite materials is the substitution of Pb^{2+} by heterovalent M^{3+} cations. A promising candidate for this type of substitution is non-toxic Bi^{3+}, which is isoelectronic with Pb^{2+}. Due to the higher charge of Bi^{3+}, bismuth ions cannot simply be incorporated into the hybrid three-dimensional $A^{1+}M^{2+}X_3$ structure of the lead-based compounds. Generally, related hybrid Bi^{3+} compounds feature low-dimensional structures resulting in less favorable optoelectronic properties than their lead-based counterparts.[15–18]

In order to incorporate Bi^{3+} ions into a three-dimensional structure, a class of materials called elpasolites, also known as double perovskites, could provide an attractive extension of the conventional perovskite system. Elpasolites, with the general formula $A_2M^{1+}M^{3+}X_6$, feature a highly symmetric cubic double perovskite structure, with one monovalent and one trivalent cation.[19] Bismuth-containing elpasolites with A = Rb, Cs, CH_3NH_3; M^{1+} = Na, K, Tl and X = F, Cl, Br have been investigated for several decades.[20–24] Unfortunately, compounds containing alkali metals do not absorb light in the visible range due to their large band gap energies (E_g) exceeding 3 eV.[20,25] Although the thallium-containing compound features a reasonable small E_g of 2.16 eV, the severe toxicity of thallium excludes this element as a non-toxic alternative for lead.[23]

Recently, several groups have reported Bi^{3+}-based double perovskites with Ag^+ as the monovalent cation featuring E_g´s of ~ 2 eV for the bromide-based material, photoluminescence (PL) lifetimes of several hundred nanoseconds and calculated charge carrier effective masses close to those calculated for methylammonium lead iodide, making it a very interesting candidate for photovoltaic applications.[19, 26–30]

However, the preparation of high quality films of these perovskites for optoelectronic applications is challenging, especially for the bromide and iodide based systems.[26] As a result of the difficulties to process this material, neither films

[a] Department of Chemistry and Center for NanoScience (CeNS), University of Munich (LMU) Butenandtstr. 5-13, 81377 Munich, Germany. E-mail: tbein@cup.uni-muenchen.de
[b] School of Electrical and Electronic Engineering, Newcastle University, Merz Court, Newcastle upon Tyne, NE1 7RU, UK

† Electronic Supplementary Information (ESI) available: See DOI: 10.1039/x0xx00000x

nor photovoltaic devices based on Ag-Bi double perovskites have been reported so far.

Since thin films are critical for making double perovskites accessible for optoelectronic applications, we have developed a synthetic route that allows for the preparation of phase pure, thin films of the double perovskite $Cs_2AgBiBr_6$. Extensive powder X-ray diffraction (PXRD) investigations revealed that high annealing temperatures of at least 250 °C are needed to remove side phases which form during the film synthesis. Light absorption measurements as well as steady-state and time-resolved PL measurements show that our films feature absorption properties and lifetimes of the photoexcited species similar to the lead-based counterparts. First steps to optimize the film synthesis conditions were undertaken to improve the optoelectronic properties of our $Cs_2AgBiBr_6$ films, leading to photovoltaic devices with PCEs of up to 2.43% and a high V_{oc} exceeding one volt. Additionally, the $Cs_2AgBiBr_6$-based devices revealed a high stability under operating conditions. Hence, we demonstrate the potential of highly tunable double perovskites as a novel class of semiconducting materials for optoelectronic applications.

Experimental

All chemicals were used as received without any further purification. All synthesis steps were conducted under ambient conditions except the application of the hole transporting layer (HTL) which was performed in a nitrogen-filled glove box.

Substrate preparation

Fluorine-doped tin oxide (FTO)-coated glass sheets (7 Ωsq^{-1}, Pilkington, USA) were patterned by etching with zinc powder and 3 M HCl. They were subsequently cleaned with a 2% Hellmanex solution and rinsed with deionized water and ethanol. Directly before applying the blocking layer, remaining organic residues were removed by an oxygen plasma treatment for 5 min. A compact titanium dioxide (TiO_2) layer was deposited by spin-coating a sol-gel precursor solution at 2000 rpm for 45 s followed by subsequent annealing at 500 °C for 45 min. For preparing the sol-gel solution, a 27.2 mM (70 µL) solution of HCl in 2-propanol (5 mL) was added dropwise to a vigorously stirred 0.43 mM (735 µL) solution of titanium isopropoxide (99.999%, Sigma–Aldrich) in 2-propanol (5 mL). Afterwards, an approx. 800 nm thick, mesoporous (mp)-TiO_2 layer was applied by spin-coating 100 µL of a TiO_2 nanoparticle paste (Dyesol DSL 18NR-T) diluted in absolute ethanol (1:2 weight ratio) onto the compact TiO_2 layer at 2500 rpm for 30 s, followed by subsequent annealing at 500 °C for 15 min under ambient conditions.

Perovskite film preparation

The precursor solution was prepared by dissolving 268 mg $BiBr_3$ (≥ 98%, Sigma Aldrich), 112.8 mg of AgBr (99.5%, Alfa Aesar) and 254 mg CsBr (99 %, Alfa Aesar) in dimethylsulfoxide (1 mL, DMSO, anhydrous, 99.9%, Sigma-Aldrich). After complete dissolution of the precursors, both the solution and the substrate were *preheated* to 75 °C before spin-coating. 100 µL of the hot precursor solution was spin-coated onto the TiO_2-covered substrate at 2000 rpm for 30 s. The substrates were subsequently *annealed* at 285 °C for 5 min under ambient conditions to allow for a complete formation of the desired double perovskite phase. The temperatures for both the *preheating* and the *annealing* steps were also varied to identify the optimal conditions for phase pure films.

Solar cell fabrication

After film formation, the films were covered with a HTL of 2,2',7,7'-tetrakis-(*N*,*N*-di-4-methoxyphenylamino)-9,9'-spirobifluorene (spiro-OMeTAD, Borun Chemicals, 99.5% purity). The HTL solution was prepared by dissolving 73 mg of spiro-OMeTAD in chlorobenzene (1 mL, 99.8%, Sigma–Aldrich). The solution was filtered and mixed with 4-*tert*-butylpyridine (10 µL, TBP, 96% Sigma Aldrich) and a 173 mg mL^{-1} bis(trifluoromethane)sulfonamide lithium salt (LiTFSI, 99.95%, Sigma–Aldrich) solution in acetonitrile (30 µL). This solution was spin-coated dynamically at 1500 rpm for 45 s. In a second step the sample rotation was accelerated to 2000 rpm for 5 s to allow the solvent to dry completely. Finally, 40 nm thick gold electrodes were thermally deposited under a high vacuum on top of the device.

Characterization

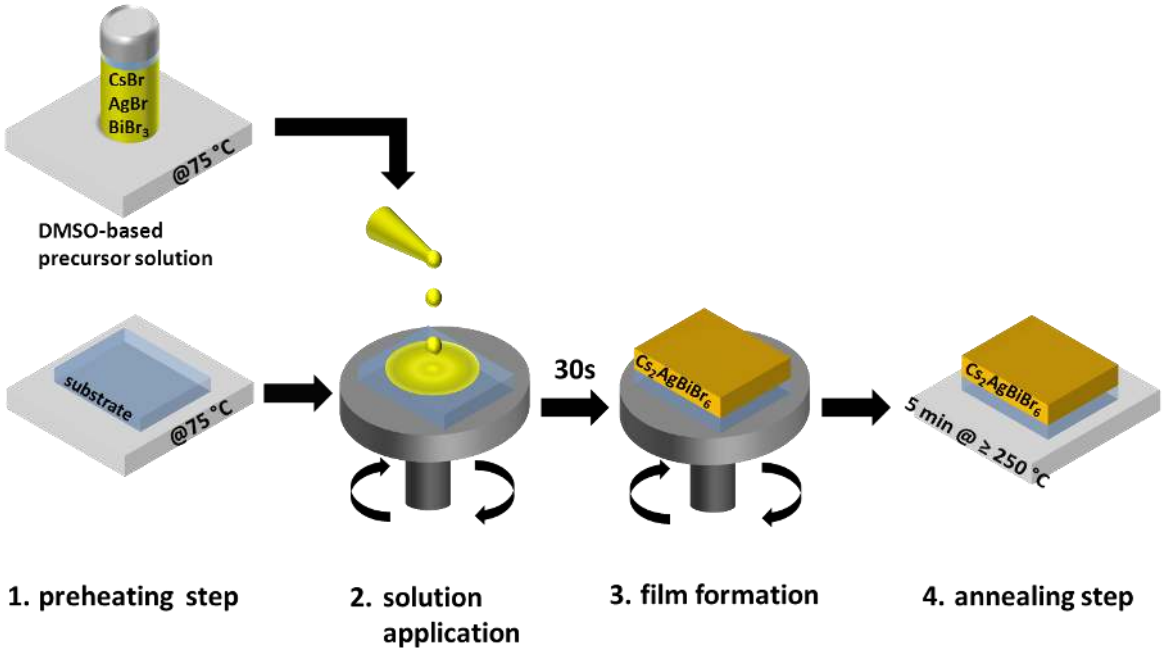

Fig. 1 Schematic of the synthesis route for $Cs_2AgBiBr_6$ thin films. The film formation (3.) occurs already while the substrate is spinning.

PXRD measurements were performed in transmission mode on a STOE Stadi MP diffractometer with a Cu Kα1 radiation source (λ = 1.54060 Å) operating at 40 kV and 40 mA. The diffractometer was equipped with a DECTRIS MYTHEN 1K solid-state strip detector. PXRD measurements on thin films were performed using a Bruker D8 Discover X-ray diffractometer operating at 40 kV and 30 mA, employing Ni-filtered Cu Kα radiation (λ = 1.5406 Å) and a position-sensitive detector (LynxEye). Scanning electron microscopy (SEM) images and EDX data were acquired on a FEI Helios NanoLab G3 UC microscope. The sample was fixed by silver paste. For the optical characterization, precursor solutions were prepared similar to those used for the devices. Similar deposition conditions were also chosen. For UV-Vis measurements the films were prepared on glass substrates or on the mp-TiO_2 substrates also used for solar cells. For PL measurements the double perovskite films were either prepared on approximately 800 nm thick mp-TiO_2 or mp-Al_2O_3 films deposited on a glass slide. For the mp-TiO_2 on glass, similar solutions and conditions were chosen as for the solar cell preparation. For the formation of the mp-Al_2O_3 film, Al_2O_3 nanoparticles dispersed in isopropanol (Sigma Aldrich, <50 nm, 20%wt) were diluted with isopropanol (Sigma Aldrich, 99.8%) in 1 : 1 ratio. 100 µL of the Al_2O_3 dispersion was spun on a glass substrate at 2500 rpm for 30 s with subsequent annealing at 120 °C for 10 min. Steady-state absorption spectra were acquired with a Lambda 1050 UV-Vis spectrophotometer (Perkin Elmer) using an integrating sphere. Steady state and time resolved PL measurements were conducted with a Fluotime 300 Spectrofluorometer (Picoquant GmbH). The excitation wavelength was fixed at 405 nm. The emission for time resolved measurements was monitored at 630 nm being the wavelength of the maximum intensity of the steady state photo-emission. *J-V* curves were recorded with a Keithley 2400 sourcemeter under simulated AM 1.5 sunlight, calibrated to 100 mW cm^{-2} with a Fraunhofer ISE certified silicon cell. The active area of the solar cells was defined with a square metal aperture mask of 0.0831 cm^2. External quantum efficiency (EQE) measurements were performed at short circuit with a bias illumination of 0.1 sun provided by an AM 1.5 solar simulator (Solar Light Model 16S). The measurements were conducted under low-frequency chopped monochromatic light (12 Hz). A 150 W xenon lamp equipped with a monochromator and order-sorting filters was used as a light source. The light intensity reaching the electrode was measured using a certified Fraunhofer ISE silicon reference cell equipped with a KG5 filter at a frequency of 40 Hz. For signal detection a Signal Recovery 7265 lock-in amplifier combined with a low-noise current amplifier (Femto DLPCA-200) was employed.

Results and Discussion

So far, bismuth halide-based double perovskite crystals have only been synthesized by solid state reactions or solution growth from the corresponding halide acids.[19,26–29] The solubility of the double perovskites in these acids is relatively low leading to double perovskite concentrations (< 0.1 M) much lower than that generally used for the preparation of lead or tin perovskite based films by solution based methods,[4–6,13,14] so it is essential to find alternative solvents that can reach a higher precursor concentration in order to prepare $Cs_2AgBiBr_6$ films from solution. Since $Cs_2AgBiBr_6$ is hardly soluble in the most commonly used solvents, we screened several alternatives where dimethylsulfoxide (DMSO) showed the highest ability to dissolve the precursors, AgBr, CsBr and $BiBr_3$, and the double perovskite (Table S1)

As a result, the $Cs_2AgBiBr_6$ films prepared in this study were deposited by spin-coating a DMSO-based precursor solution on top of a substrate. Our utilized synthesis route employs two different heating steps. The first step is named "preheating step" where the substrate and precursor solution are heated to 75 °C prior the spin-coating. Then, the hot precursor solution was spun on top of the hot substrate. This preheating step improves the surface coverage and film quality (Fig. S1). The second heating step named "annealing step", is performed after the spin-coating procedure at a temperature of at least 250 °C and is needed to obtain phase pure films. A scheme of the complete synthesis procedure is given in Fig. 1. Previous studies by Xiao *et al.* propose the facile formation of side phases due to the narrow chemical potential region for the formation of phase-pure $Cs_2AgBiBr_6$, which could have negative effects on the optoelectronic properties of the double perovskite.[31] Therefore, we performed temperature-dependent PXRD investigations to assure the formation of phase-pure films. We found that two of the predicted side phases, namely $Cs_3Bi_2Br_9$ and AgBr,[31] actually formed during the film synthesis. In order to remove these side phases we performed an extensive annealing temperature study, revealing that an annealing temperature of at least 250 °C is needed to assure complete conversion of the precursors to the desired double perovskite phase. Fig. 2a & b depict PXRD patterns of $Cs_2AgBiBr_6$ powders obtained from $Cs_2AgBiBr_6$ films at different annealing temperatures showing the typical reflections of the cubic elpasolite structure.[26] The patterns from samples annealed at temperatures below 250 °C feature additional reflections at 12.8°, 30.9° and 44.2°, which can be assigned to $Cs_3Bi_2Br_9$ and AgBr, while films annealed at 250 °C appear to be phase-pure. This trend can also be confirmed with the corresponding PL spectra were only the 250 °C sample exhibits the typical PL signal of $Cs_2AgBiBr_6$ (Fig. S2). The PXRD patterns in Fig. 2, clearly show that the vanishing of the side-phases is not caused by the removal of metal-solvent intermediates, as it was shown for lead and tin based hybrid perovskites.[32,33] This is also supported by the evolution of the intensity of the reflections of the side-phases with temperature. Even at 150 °C annealing temperature, which is usually sufficient to remove the metal-solvent intermediates, no decrease of the reflection intensities could be observed pointing to highly stable side phases. However, McClure *et al.* demonstrated the synthesis of $Cs_2AgBiBr_6$ via solid state reaction at 210 °C for 10 h,[19] which is close to the temperature we use to obtain phase pure double perovskite films. Therefore, we hypothesize that micro scale solid state reactions in our prepared films are responsible for the complete conversion of the precursors and side-phases into the desired $Cs_2AgBiBr_6$ phase.

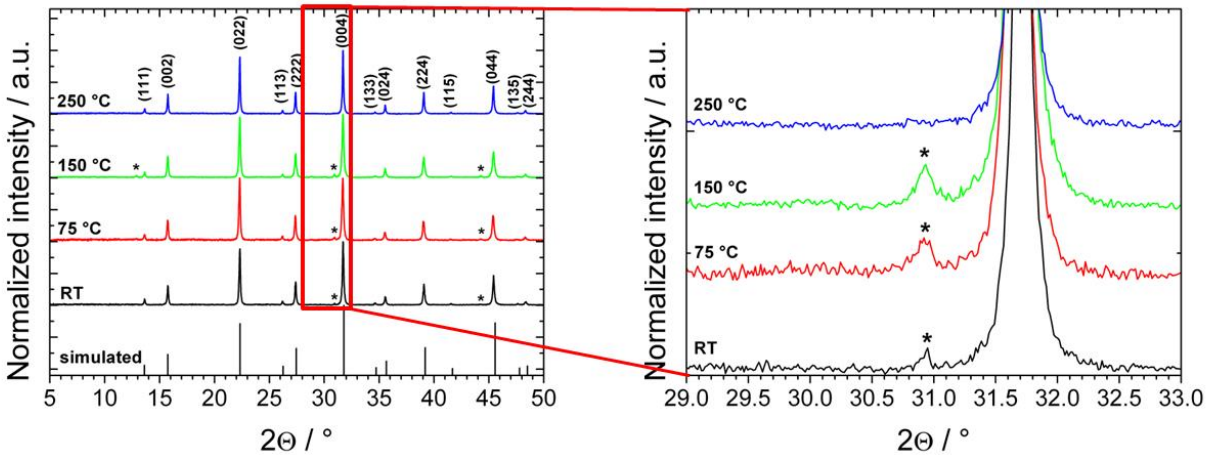

Fig. 2. (a, b) XRD patterns of $Cs_2AgBiBr_6$ powders obtained from our prepared films annealed at different temperatures, the asterisk (*) indicates the position of reflections from the side phases AgBr (ICDD No. 00-006-0438) and $Cs_3Bi_2Br_9$ (ICDD No. 01-070-0493), respectively. The sample labelled with RT was kept at room temperature (ca. 25 °C) after film formation without any annealing step.

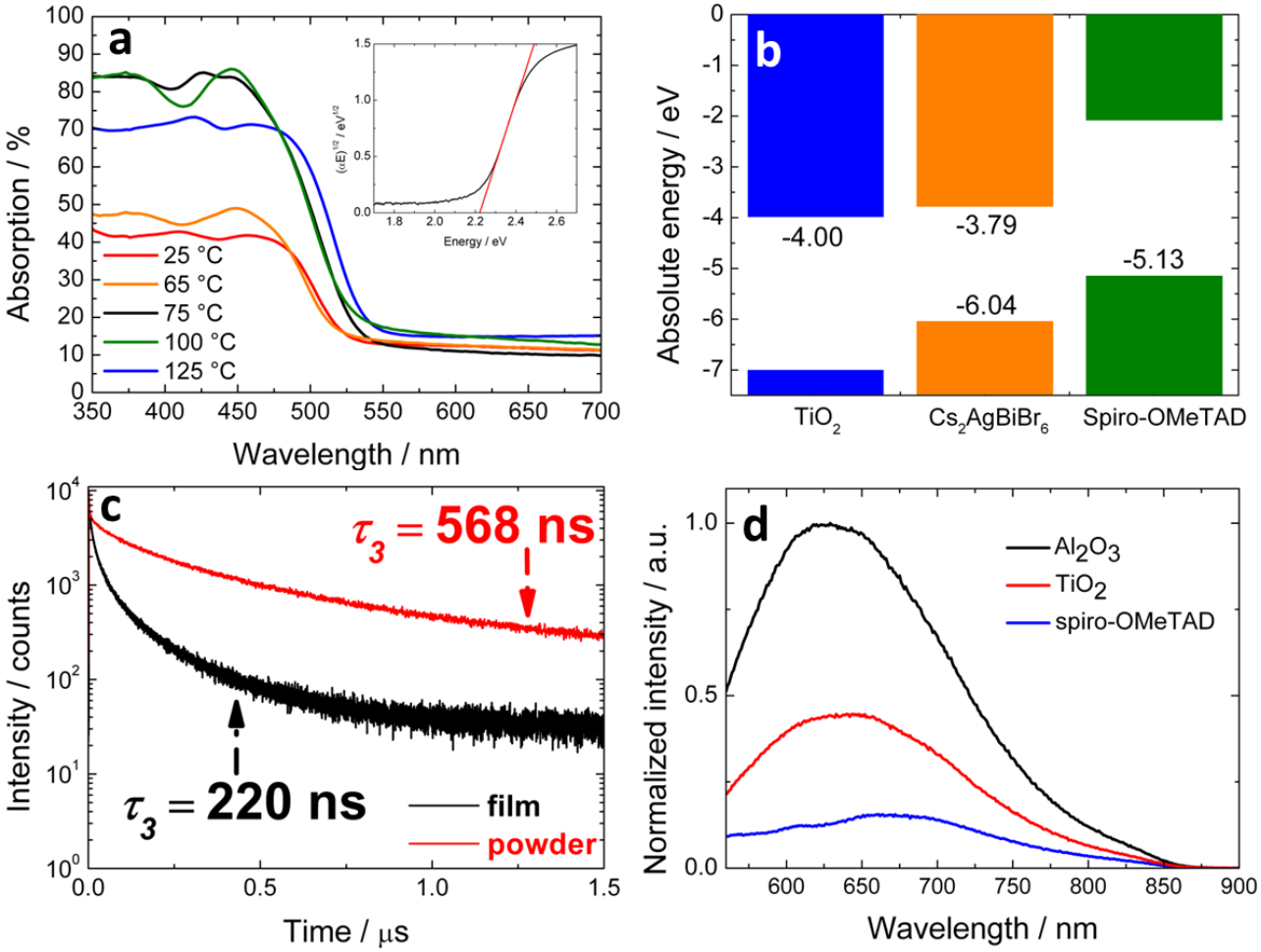

Fig. 3 (a) Optical absorption spectra of $Cs_2AgBiBr_6$ films prepared from DMSO on flat glass substrates. The films were manufactured without a preheating step at room temperature (ca. 25 °C) or with a preheating step at 65 °C, 75 °C, 100 °C or 125 °C before spin-coating. (b) Energy level diagram of the double perovskite and the charge extraction materials.[26] (c) TCSPC decays of a $Cs_2AgBiBr_6$ film on glass and polycrystalline powder. (d) PL emission spectra of $Cs_2AgBiBr_6$ films on mp-Al_2O_3, mp-TiO_2 and mp-Al_2O_3 covered with spiro-OMeTAD. The films presented in 3d were prepared on an 800 nm thick mp scaffold. All films were prepared according the procedure depicted in Fig. 1 with a 285 °C annealing step.

As the $Cs_2AgBiBr_6$ films were prepared for photovoltaic applications, sufficient light absorption is mandatory for efficiently working devices. In order to optimize the optical absorption properties of the double perovskite films, we added an additional preheating step to our synthesis protocol where the spin-coating solution and the substrate were put on a hotplate and heated to 75 °C before spin-coating. Fig. 3a shows absorption spectra of $Cs_2AgBiBr_6$ films on glass prepared with and without a preheating step at different temperatures. Without the preheating step, insufficient light absorption would limit the photocurrent of the resulting devices to approximately 2 mA cm^{-2}, which is inadequate to prepare efficient solar cells. We found that preheating the substrate and the solution increases the quality of the double perovskite films, by improving the surface coverage, as can be seen with the naked eye, enhancing the optical absorption of the films (Fig. S1). In particular, the absorption close to the onset is significantly increased, which is also observable for films made on an mp-TiO_2 scaffold as used for solar cell fabrication (Fig. S3). We attribute the increase of the optical absorption to an increased surface coverage on the substrate due to a larger amount of deposited double perovskite caused by the faster solvent evaporation at elevated temperatures. Increasing the amount of deposited $Cs_2AgBiBr_6$ by simply increasing the concentration of the precursors in the spin-coating solution is not possible since the precursor concentration of the utilized solution is already close to the maximum of about 0.6 M.

The band gap of the $Cs_2AgBiBr_6$ films was determined from the absorption spectra given in Fig. 3a. The spectra show a steep onset at about 550 nm corresponding to an E_g of 2.21 eV for a direct band gap obtained with a Tauc plot (see inset), which is comparable to the value reported by McClure *et al.*[19] and consistent with other reports ranging from 1.83 eV[26] to 2.19 eV[19]. The relatively large spread of the reported E_g values most likely originates from different synthesis conditions and measurement methods used in the different studies.[29] According to the Shockley-Queisser limit, a theoretical maximum PCE of 16.4% can be obtained with an E_g of 2.2 eV, thus holding promise for working double perovskite based photvoltaics.[34] Although, the theoretical maximum PCE of this

material does not reach the highest reported PCEs of single junction methylammonium lead iodide ($MAPbI_3$) based photovoltaics, $Cs_2AgBiBr_6$ is a promising candidate for applications in tandem solar cells as it was already shown for methylammonium lead bromide, which features a slightly larger E_g of 2.3 eV.[35]

The energy level diagram in Fig. 3b[26] shows that the conduction band (CB) of the $Cs_2AgBiBr_6$ is well aligned with the CB of the electron transporting material (ETM) titania, which was also recently shown in a computational study of Feng *et al*.[36] In contrast, the highest occupied molecular orbital (HOMO) of the hole transporting material (HTM) 2,2',7,7'-tetrakis-(N,N-di-4-methoxyphenylamino)-9,9'-spirobifluorene (spiro-OMeTAD) shows a strong offset compared to the valence band (VB) of the double perovskite, which is likely to limit the potential V_{oc} of a photovoltaic device. In this work, as a first demonstration of the potential of $Cs_2AgBiBr_6$, we focused on the preparation of devices comprising this state-of-the-art material which has been shown to be able to reach V_{oc}'s exceeding 1.5V.[37] Nevertheless, the energy level alignment allows for charge extraction, and functioning devices are expected.

Not only the band gap and energy alignment with the charge extraction layers, but also charge collection efficiency is important to fabricate high-efficiency solar cells. PL lifetime measurements can provide an indication as to whether a material can perform in this area. Here, we investigated the PL decay times of the double perovskite films by time-correlated single photon counting (TCSPC). For comparison, additional TCSPC measurements were performed on polycrystalline powder samples that were obtained by the conventional approach from HBr solution.[26] The PL decays are displayed in Fig. 3c. Although the PL of $Cs_2AgBiBr_6$ features three differently fast decay processes, only the value for the long-lived process is given in Fig. 3c. We attribute the two short lifetime processes to trap and/or surface state emission, while the long lifetime process is suggested to be the fundamental PL decay time of the material.[26] Both the powder and the film show long PL decay times in the range of hundreds of nanoseconds, similar to the values observed for lead-based hybrid perovskites,[38] hinting at the potential for well-performing devices. We note that the decay times do not differ significantly between single crystals and polycrystalline powders, which suggest a high defect tolerance of this material.[26] The slightly faster decay for films is likely the result of a larger concentration of trap states in the perovskite film, as has been previously shown for lead halide-based films.[39] Here, the fast formation of the perovskite during the spin-coating process causes a broad grain size distribution within the film and, consequently, a large number of grain boundaries.

PL quenching experiments are widely used to study the charge transfer from a photoabsorber to the charge-selective contacts.[40,41] From the energy diagram (Fig. 3b) we expect favorable charge transfer behavior from $Cs_2AgBiBr_6$ to the electrodes, which was experimentally tested with PL quenching experiments. For the measurements, mp-TiO_2 and spiro-OMeTAD were chosen as ETM and HTM, respectively, while mp-Al_2O_3 was used as reference as no charge transfer is expected (for experimental details see the characterization section). Fig. 3d shows the quenching of the PL emission of $Cs_2AgBiBr_6$ on TiO_2 by approximately 60%, while the PL was reduced by more than 80% in contact with spiro-OMeTAD. These results indicate that charge transfer from the double perovskite to the charge-selective materials is taking place, as required for working photovoltaic devices. However, the low PL quantum yield of $Cs_2AgBiBr_6$ indicates that the main recombination pathways in $Cs_2AgBiBr_6$ are nonradiative[26] and therefore not detectable in PL quenching experiments. It has to be mentioned that, the PL signal of our films is relatively broad but similar to that reported for single crystals.[26] The broad PL signal is most likely caused by defects and excitonic effects.[29] Furthermore, previous studies by Slavney *et al.* revealed that in addition to the direct band gap at about 2.2 eV, $Cs_2AgBiBr_6$ features an indirect band gap at about 1.9 eV, which was not detectable in the light absorption spectra of our prepared films.[26] Considering that the value of the indirect band gap matches quite closely the position of the observed PL maximum, we believe that the relatively large red shift of the maximum of the PL signal with respect to the

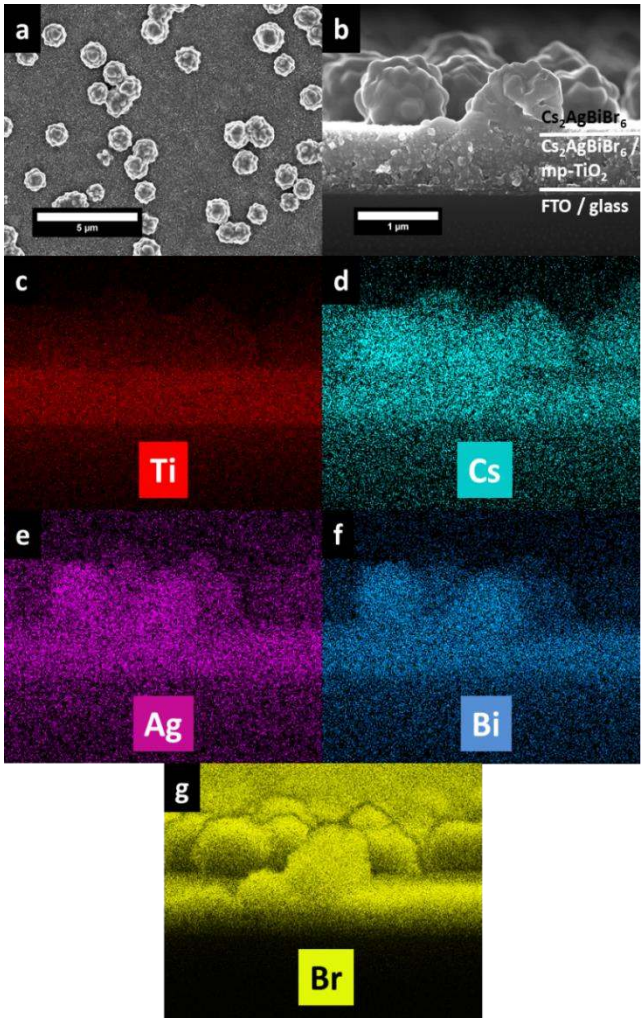

Fig. 4 (a) SEM top-view image of a $Cs_2AgBiBr_6$ film prepared with a 75 °C preheating step on mp-TiO_2. (b) SEM cross-section image of the film presented in (a). (c-g) EDX elemental maps of Ti (red), Cs (turquoise), Ag (purple), Bi (blue) and Br (yellow).

absorption onset can be assigned to contributions of this indirect band gap at about 1.9 eV. Nevertheless, the PL results indicate that $Cs_2AgBiBr_6$ films can be incorporated in working photovoltaic devices.

The morphology of the double perovskite films prepared according the procedure shown in Fig. 1 was investigated with scanning electron microscopy (SEM). Fig. 4a shows a SEM top-view image of a $Cs_2AgBiBr_6$ film, on an 800 nm thick mp-TiO_2 scaffold as used for the preparation of photovoltaic devices. Here, no dense and homogeneous capping layer on top of the mp-TiO_2 is observable, instead many agglomerates at the scale of about one micron have formed. This is most likely caused by the fast crystallization process during the spin-coating procedure induced by fast solvent evaporation due to the performed preheating step, as shown in Fig. 1. We believe that this fast crystallization process impedes homogeneous crystal growth, leading to the observed agglomerates. Energy dispersive X-ray spectroscopy (EDX) measurements were performed to evaluate the penetration depth of the double perovskite into the mp-TiO_2 scaffold. Fig. 4b-g show a SEM cross-section of the film presented in Fig. 4a and the elemental maps of Ti, Cs, Ag, Bi and Br, respectively. The cross-section image and EDX maps clearly establish complete infiltration of $Cs_2AgBiBr_6$ into the mp-TiO_2 scaffold, which is important to obtain efficient devices, while some additional $Cs_2AgBiBr_6$ agglomerates are formed on top of the scaffold.

Based on the promising results of the above investigations, we incorporated the newly developed $Cs_2AgBiBr_6$ films into photovoltaic devices featuring a layer assembly of fluorine doped tin oxide (FTO)/dense TiO_2/mp-TiO_2/$Cs_2AgBiBr_6$/spiro-OMeTAD/Au to investigate their photovoltaic characteristics. As mentioned before, the thickness of the utilized mp-TiO_2 layer was approx. 800 nm as depicted in Fig. 4b.

Fig. 5a displays the statistical parameter distribution of 48 solar cells (per treatment temperature) that were assembled with $Cs_2AgBiBr_6$ films prepared without a preheating step and with a preheating step at different temperatures. The studies revealed a PCE maximum at 75 °C, we attribute to the improved optical properties of those films shown in Fig. 3a and S3. Furthermore, the *J-V* curves given in Fig. S4 show that the increased device performance at 75 °C preheating is not only caused by an increased short-circuit current (J_{sc}) due to the enhanced optical absorption properties because of the preheating, but also by the enhanced fill factor (FF) and by the V_{oc} increase observed with increasing preheating temperature. We hypothesize that the preheating also improves the mp-TiO_2/double perovskite

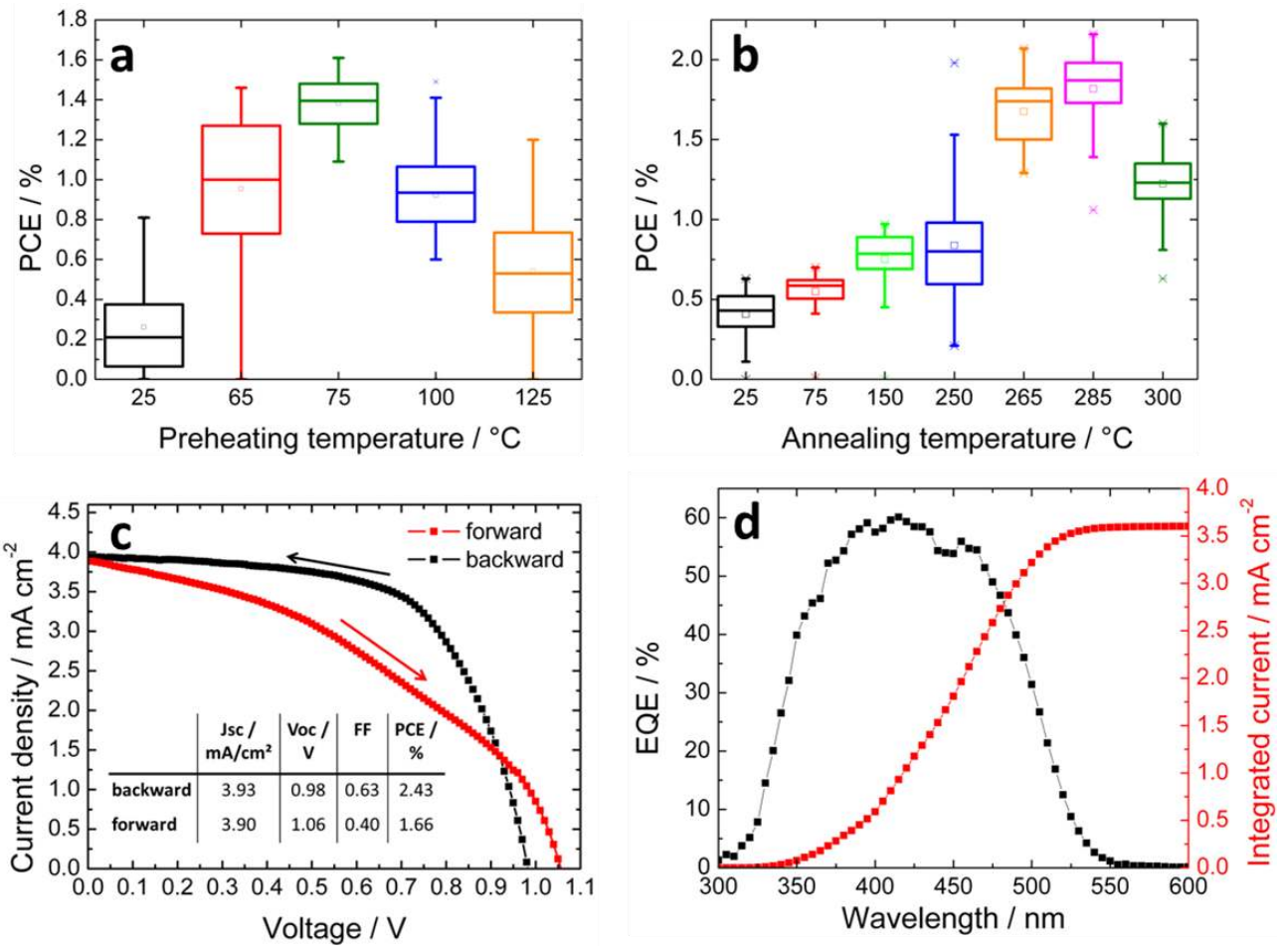

Fig. 5 (a) Device performance as a function of preheating temperature, values obtained from 48 individual devices per temperature. All films were annealed at 250 °C after spin-coating to achieve phase pure $Cs_2AgBiBr_6$ films. (b) Device performance of solar cells assembled with $Cs_2AgBiBr_6$ films preheated at 75 °C as a function of annealing temperature, values obtained from 48 individual devices per temperature. (c) *J-V* curve of the best performing device (d) EQE spectrum (black) and integrated predicted current (red) of a device showing a J_{sc} of 3.7 mA cm^{-2}.

interface, for e.g. by reducing trap states, resulting in an enhanced performance.[42] The large spread of the device performance observable for films preheated at 25 °C and 65 °C indicates that the improvement of the TiO_2/double perovskite interface is not as reliable as for preheating at 75 °C, which results in the smallest performance spread of all investigated preheating temperatures. The PCE decrease and the broadening of the PCE distribution at higher preheating temperatures (>100 °C) is tentatively attributed to the formation of a top layer consisting of large crystallites on the mp-TiO_2 scaffold, caused by a strongly accelerated precipitation of the double perovskite due to the relatively high deposition temperature, as shown in Fig. S5, which is apparently too thick for efficient charge transport. We note that $Cs_2AgBiBr_6$ films prepared without a preheating step feature the most homogeneous morphology, with the lowest number of agglomerates on top the mp-TiO_2 scaffold (see Fig S6), without resulting in the best performing devices. Accordingly, it is likely that preheating to 75 °C results in double perovskite films featuring strongly improved optoelectronic properties, which overcome the possible detrimental effects of a less homogeneous morphology due to the agglomerate formation on top of the mp-TiO_2 induced by the preheating.

Although a full conversion of the precursors into the double perovskite phase is achieved by 250 °C annealing after film formation, the obtained PCEs showed a large spread. Therefore, an extensive study of the influence of the annealing temperature on device performance was conducted. Fig. 5b shows the relation between annealing temperature and the statistical distribution of PCEs of 48 individual devices. The highest and most reproducible PCEs were obtained for an annealing temperature of 285 °C. The increase in PCE with increasing annealing temperature is dominated by an increase of J_{sc} and FF at annealing temperatures below 250 °C, whereas only the J_{sc} rises significantly at higher annealing temperatures (Fig. S7). Up to 250 °C, this trend is most likely caused by a decrease of the side phases observed in the PXRD pattern (Fig. 2a & b), until the phase-pure $Cs_2AgBiBr_6$ has formed at 250 °C. This temperature is the lower end of the range of the annealing temperature required to fully convert the precursors into the double perovskite phase. Annealing at slightly higher temperatures (285 °C) make this process more robust, leading to slightly higher PCEs and more importantly, better reproducibility. The decrease in PCE at even higher temperature (300 °C) is associated with a reduction in J_{sc}, which we attribute to the degradation of the $Cs_2AgBiBr_6$ films as the double perovskite slowly starts to come off the substrate at annealing temperatures at about 300 °C (Fig. S7).

The application of our optimized synthesis conditions resulted in devices showing PCEs of more than two percent. Remarkable is the relatively narrow distribution in the performance, taking into consideration the surface of the film that contains the perovskite agglomerates. Fig. 5c displays the *J-V* curve of the best performing device exhibiting a PCE of 2.43%. In particular, the V_{oc} of 0.98 V is significantly higher than that of other bismuth-based compounds featuring comparable *Eg´s*.[43-45] Moreover, V_{oc}´s exceeding 1 V were measured, which are, with the best of our knowledge, the highest V_{oc} values reported for bismuth halide based materials (see Fig. S7), confirming the good alignment of the conduction band of the perovskite with TiO_2 as predicted from the energy level diagram in Fig. 3b and in computational studies.[36]

These PCEs are viewed as an excellent starting point for double perovskite absorbers in solar cells if one considers that the spectroscopically predicted maximum efficiency of $Cs_2AgBiBr_6$ is reaching 7.92% determined from density functional theory calculations by Savory *et al*..[46] As the band gap of $Cs_2AgBiBr_6$ is 2.2 eV, the current of solar cells comprising this absorber is limited to ~6.8 mA cm^{-2} under 1 sun illumination. External quantum efficiency (EQE) measurements show an integrated current of 3.6 mA cm^{-2} (Fig. 5d), which is in good agreement with the J_{sc} of 3.7 mA cm^{-2} obtained from the *J-V* curve (Fig. S8). The EQE spectrum (Fig. 5d) shows an onset around 550 nm, which is in agreement with the absorbance data, and is above 50% from 375 to 470 nm with a maximum of 60% at 415 nm. According to Fig. 5c the *J-V* curves show hysteresis, comparable to behavior observed in devices employing lead-based perovskites.[47–50] Computational studies by Eames *et al*. reveal that the migration of the halide anions contributes to the hysteresis in hybrid lead halide perovskite based photovoltaics due to their very low activation barrier.[51] Therefore, we believe that similar effects, including trapping/de-trapping of charge carriers,[47, 52] are likely to be responsible for the hysteresis in our $Cs_2AgBiBr_6$ based devices since the crystal structure of the double perovskite is very similar.

Besides performance, stability is also an important issue for widespread applications as devices need to work for many years at high intensity illumination. Accordingly, we conducted the first stability studies on $Cs_2AgBiBr_6$-based solar cells. Fig. 6a displays the stabilized power output under ambient conditions. The device shows a rapid response after illumination, resulting in a PCE of around 2.0%. During the next 30 s, only a very small decay of around 5% in the PCE was observed, after which the PCE stabilizes just above 1.9% and no further decay was observed over a period of five minutes, indicating a similar performance stability like lead halide based solar cells. Another device was illuminated using an AM1.5 solar simulator under ambient conditions for a period of 100 min while at regular intervals *J-V* scans were taken (Fig 6b & S9). During the first couple of minutes an increase in the PCE was observed as a result of an increase in the V_{oc}, which we assign to light soaking effects.[53] This indicates the presence of (interfacial) defects that can be neutralized with photogenerated charge carriers.[53–59] After this period the V_{oc} and J_{sc} turn out to be very stable. Some fluctuation in the FF (Fig. S9) are observed, which are also reflected in the PCE, nevertheless after 100 min the PCE did not significantly decay and at 2.06%, it was even higher than the initial value measured before the light soaking. The results presented in Figure 6b & S9 indicate a high device stability under permanent illumination, higher than that of reported $MAPbI_3$ based devices showing a significant drop of J_{sc} within the first two hours.[60] Furthermore, initial longer-term stability studies on the new $Cs_2AgBiBr_6$-based devices revealed an excellent stability under ambient conditions for at least 25 days

(Fig. S10). The devices were stored in the dark to avoid any possible light driven degradation processes of the double perovskite as indicated by Slavney *et al*..[26]

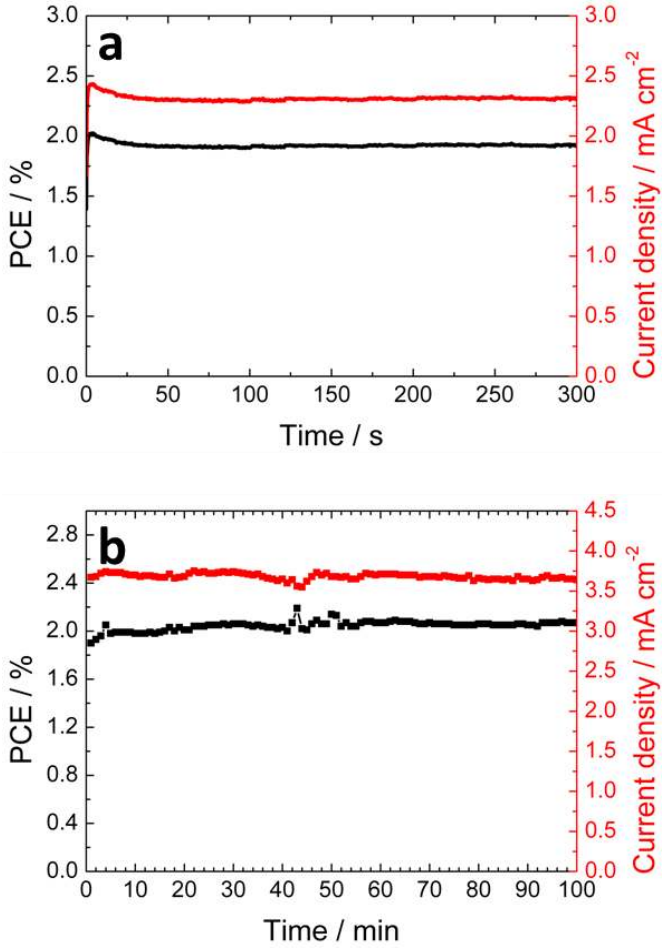

Fig. 6 (a) Stabilized power output and current density measured under ambient conditions without encapsulation. (b) Photovoltaic performance as a function of time under continuous illumination under ambient conditions. All devices were manufactured according the procedure described in Fig. 1 with a 285 °C annealing step.

Conclusions

In conclusion, we have demonstrated the solution-based formation of double perovskite films via a fast and efficient spin-coating method. Extensive studies of the synthesis conditions revealed the necessity of a high-temperature annealing step to fully convert the precursors into the desired double perovskite phase, and the requirement of an additional preheating step to improve the optical properties of the $Cs_2AgBiBr_6$ films. The resulting $Cs_2AgBiBr_6$ films feature an E_g comparable to that of single crystals and polycrystalline powders, and solar cells comprising these new films exhibit very promising PCEs close to 2.5% with V_{oc}´s exceeding one volt, demonstrating the suitability of double perovskites for optoelectronic devices. Furthermore, our $Cs_2AgBiBr_6$-based devices feature a high stability under constant illumination at ambient conditions, higher than that of reported $MAPbI_3$ based solar cells. Since the elpasolite structure allows for numerous different combinations of elements, this work shows the potential for developing a wide range of double perovskites for diverse environmentally friendly optoelectronic applications.

Conflict of interests

There are no conflicts to declare.

Acknowledgements

We thank Julian Rotter from the Chemistry Department of the University of Munich (LMU) for the scanning electron microscopy and energy dispersive x-ray scattering measurements. We acknowledge funding by the Bavarian State Ministry of the Environment and Consumer Protection, the Bavarian network “Solar Technologies Go Hybrid”, the DFG Excellence Cluster Nanosystems Initiative Munich (NIM), the German Federal Ministry of Education and Research (BMBF) under the Project ID 03SF0516B and the EPSRC (EP/P03148X/1). We gratefully acknowledge support from the European Union through the award of a Marie Curie Intra-European Fellowship.

Notes and references

1 M. M. Lee, J. Teuscher, T. Miyasaka, T. N. Murakami and H. J. Snaith, *Science*, 2012, **338,** 643–647.
2 NREL chart, http://www.nrel.gov/ncpv/images/efficiency_chart.jpg, (accessed July 2017).
3 T. M. Brenner, D. A. Egger, L. Kronik, G. Hodes and D. Cahen, *Nat. Rev. Mater*., 2016, **1,** 15007.
4 S. De Wolf, J. Holovsky, S.-J. Moon, P. SLoiper, B. Niesen, M. Ledinsky, F.-J. Haug, Yum and C. Ballif *J. Phys. Chem. Lett*., 2014, **5,** 1035−1039.
5 S. D. Stranks, G. E. Eperon, G. Grancini, C. Menelaou, M. J. P. Alcocer, T. Leijtens, L. M. Herz, A. Petrozza and H. J. Snaith *Science*, 2013, **342,** 341−344.
6 C. Wehrenfennig, G. E. Eperon, M. B. Johnston, H. J. Snaith and L- M. Herz, *Adv. Mater*., 2014, **26,** 1584−1589.
7 R. E. Brandt, V. Stevanović, D. S. Ginley and T. Buonassisi, *MRS Commun*., 2015, **5,** 265−275.
8 A. Walsh, D. O. Scanlon, S. Chen, X. G. Gong and S.-H. Wei, *Angew. Chem., Int. Ed*., 2015, **54,** 1791−1794.
9 Y.-Y Zhang, S. Chen, P. Xu, H. Xiang, X.-G. Gong, A. Walsh and S.-H. Wei, *arXiv:1506.01301*, 2015.
10 G. P. Nagabhushana, R. Shivaramaiah and A. Navrotsky, *Proc. Natl. Acad. Sci. U. S. A*., 2016, **113,** 7717−7721.
11 N. Aristidou, I. Sanchez-Molina, T. Chotchuangchutchaval, M. Brown, L. Martinez, T. Rath and S. A. Haque, *Angew. Chem., Int. Ed.*, 2015, **54,** 8208−8212.
12 Babayigit, A.; Ethirajan, A.; Muller, M.; Conings, B. *Nat. Mater*., **2016,** *15,* 247−251.
13 F. Hao, C. C. Stoumpos, D. H. Cao, R. P. H. Chang and M. G. Kanatzidis, *Nat. Photonics*, 2014, **8,** 489–494.
14 N. K. Noel, S. D. Stranks, A. Abate, C. Wehrenfennig, S. Guarnera, A. A. Haghighirad, A. Sadhanala, G. E. Eperon, S. K. Pathak, M. B. Johnston, A. Petrozza, L. M. Herz and H. J. Snaith, *Energy Environ. Sci.*, 2014, **7,** 3061–3068.
15 R. Jakubas, J. Zaleski and L. Sobczyk, *Ferroelectrics*, 1990, **108**, 109−114.

16 S. Sun, S. Tominaka, J-H. Lee, F. Xie, P. D. Bristowe, A. K. Cheetham, *APL Mater*., 2016, **4,** 031101.
17 B. Chabot and E. Parthé, *Acta Cryst.*, 1978, **B34,** 645–648.
18 A. J. Lehner, D. H. Fabini, H. A. Evans, C. A. Hébert, S. R. Smock, J. Hu, H. Wang, J. W. Zwanziger, M. I. Chabinyc and R. Seshadri, R. *Chem. Mater*., 2015, **27,** 7137–7148.
19 E. T. McClure, M. R. Ball, W. Windl and P. M. Woodward, *Chem. Mater*., 2016, **28,** 1348−1354.
20 L. R. Morrs and W. R. Robinson, *Acta Crystallogr., Sect. B: Struct. Crystallogr. Cryst. Chem.*, 1972, **28,** 653−654.
21 F. Pelle, B. Jacquier, J. Denis and B. J. Blanzat, *Lumin*., 1978, **17,** 61−72.
22 W. Smit, G. Dirksen and D. Stufkens, *J. Phys. Chem. Solids.*, 1990, **51,** 189−196.
23 Z. Deng, F. Wei, S. Sun, G. Kieslich, A. K. Cheetham and P. D. Bristowe, *J. Mater. Chem.*, *A* 2016, **4,** 12025−12029.
24 A. Tressaud, S. Khaïroun, J. P. Chaminade and M. Couzi, *Phys. Status Solidi A* 1986, ***98,*** 417–421.
25 F. Wei, Z. Deng, S. Sun, F. Xie, G. Kieslich, D.M. Evans, M. A. Carpenter, P. D. Bristowe and A. K. Cheetham, *Mater. Horiz*., 2016, **3,** 328−332.
26 A. H. Slavney, T. Hu, A. M. Lindenberg and H. I. Karunadasa, *J. Am. Chem. Soc.*, 2016, **138,** 2138−2141.
27 G. Volonakis, M. R. Filip, A. A. Haghighirad, N. Sakai, B. Wenger, H. J. Snaith, and F. Giustino, *J. Phys. Chem. Lett.*, 2016, **7,** 1254−1259.
28 F. Wei, Z. Deng, S. Sun, F. Zhang, D. M. Evans, K. Kieslich, S. Tominaka, M. A. Carpenter, J. Zhang, P. D. Bristowe and A. K. Cheetham, *Chem. Mat*., 2017, **29,** 1089‑1094.
29 M. R. Filip, S. Hillman, A. A. Haghighirad, H. J. Snaith and F. Giustino, *J.Phys.Chem.Lett*., 2016, **7,** 2579−2585.
30 M. R. Filip, C. Verdi and F. Giustino, *J. Phys. Chem. C*, 2015, **119**, 25209–25219.
31 Z. Xiao, W. Meng, J. Wang and Y. Yan, *ChemSusChem*, 2016, **9,** 2628–2633.
32 N. J. Jeon, J. H. Noh, Y. C. Kim, W. S. Yang, S. Ryuand and S. I. Seok, *Nat. Mater.*, 2014, **13,** 897–903.
33 F. Hao, C. C. Stoumpos, P. Guo, N. Zhou, T. J. Marks, R. P. H. Chang and M. G. Kanatzidis, *J. Am. Chem. Soc.*, 2015, **137,** 11445−11452
34 S. Rühle, *Phys. Status Solidi A*, 2017, 1600955.
35 R. Sheng, A. W. Y. Ho-Baillie, S. Huang, M. Keevers, X. Hao, L. Jiang, Y.-B Cheng, and M. A. Green, *J. Phys. Chem. Lett.*, 2015, **6,** 3931–3934.
36 H.-J. Feng, W. Deng, K. Yang, J. Huang and X. C. Zeng, *J. Phys. Chem. C*, 2017, **121,** 4471–4480.
37 S. Gholipour, A. M. Ali, J.-P. Correa-Baena, S.-H. Turren-Cruz, F. Tajabadi, W. Tress, N. Taghavinia, M. Grätzel, A. Abate, F. De Angelis, C. A. Gaggioli, E. Mosconi, A. Hagfeldt and M. Saliba, *Adv. Mater.*, 2017, 1702005.
38 D. Shi, V. Adinolfi, R. Comin, M. Yuan, E. Alarousu, A. Buin, Y. Chen, S. Hoogland, A. Rothenberger, K. Katsiev, Y. Losovyj, X. Zhang, P. A. Dowben O. F. Mohammed, E. H. Sargent and O. M. Bakr, *Science*, 2015, **347,** 519–522.
39 D. W. deQuilettes, S. M. Vorpahl, S. D. Stranks, H. Nagaoka, G. E. Eperon, M. E. Ziffer, H. J. Snaith, D. S. Ginger, *Science,* 2015, aaa5333.
40 D. S. Ginger and N. C. Greenham, *Phys. Rev. B*, 1999, **59,** 10622–10629.
41 P. Docampo, J. M. Ball, M. Darwich, G. E. Eperon and H. J. Snaith, *Nat. commun*., 2013, **4,** 2761.
42 M. Abdi-Jalebi, M. I. Dar, A. Sadhanala, S. P. Senanayak, F. Giordano, S. M. Zakeeruddin, M. Grätzel and R. H. Friend, *J. Phys. Chem. Lett.*, 2016, **7,** 3264–3269.
43 Y. Kim, Z. Yang, A. Jain, O. Voznyy, G.-H. Kim, M. Liu, L. N. Quan, F. p. García de Arquer, R. Comin, J. Z. Fan and E. H. Sargent, *Angew. Chem., Int. Ed.*, 2016, **55,** 9586–9590.
44 B.-W. Park, B. Philippe, X. Zhang, H. Rensmo, G. Boschloo and E. M. Johansson, *J. Adv. Mater.*, 2015, **27,** 6806–6813.
45 I. Turkevych, S. Kazaoui, E. Ito, T. Urano, K. Yamada, H. Tomiyasu, H. Yamagishi, M. Kondo and S. Aramaki, *ChemSusChem*, 2017, *10,* 1–7.
46 C. N. Savory, A. Walsh and D. O. Scanlon, *ACS Energy Lett.*, 2016, **1,** 949–955.
47 H.J. Snaith, A. Abate, J. M. Ball, G. E. Eperon, T. Leijtens, N. K. Noel, S. D. Stranks, J. T. W. Wang, K. Wojciechowski and W. Zhang, *J. Phys. Chem. Lett.*, 2014, **5,** 1511–1515.
48 E. L. Unger, E. T. Hoke, C. D. Bailie, W. H. Nguyen, A. R. Bowring, T. Heumüller, M. G. Christoforo and M. D. McGehee, *Energy Environ. Sci*., 2014, **7,** 3690–3698.
49 H. S. Kim and N. G. Park, *J. Phys. Chem. Lett*., 2014, **5,** 2927–2937.
50 R. S. Sanchez, V. Gonzalez-Pedro, J. W. Lee, N. G. Park, Y. S. Kang, I. Mora-Sero and J. Bisquert, *J. Phys. Chem. Lett.*, 2014, **5,** 2357–2363.
51 C. Eames, J. M. Frost, P. R. F. Barnes, B. C. O´Regan, A. Walsh and M. S. Islam, *Nat. Commun.*, 2015, 7497.
52 A. Dualeh, T. Moehl, N. Tétreault, J. Teuscher, P. Gao, M. K. Nazeeruddin and M. Grätzel, *ACS Nano*, 2013, **8,** 362–373.
53 C. Zhao, B. Chen, X. Qiao, L. Luan, K. Lu and B. Hu, *Adv. Energy Mater.*, 2015, ***5,*** 1500279.
54 P. Tiwana, P. Docampo, M. B. Johnston, L. M. Herz and H. J. Snaith, *Energy Environ. Sci*., 2012, ***5,*** 9566–9573.
55 L. Cabau, L. Pellejà, J. N. Clifford, C. V. Kumar and E. Palomares, *J. Mater. Chem. A*, **2013,** *1*(31), 8994–9000.
56 T. Kobayashi, H. Yamaguchi and T. Nakada, *Prog. Photovolt: Res. Appl.*, 2014, ***22,*** 115–121.
57 L. Yang, B. Xu, D. Bi, H. Tian, G. Boschloo, L. Sun and E. M. Johansson, *J. Am. Chem. Soc.*, 2013, ***135,*** 7378–7385.
58 J. Kim, G. Kim, Y. Choi, J. Lee, S. Heum Park and K. Lee, *Appl. Phys.*, 2012, **111,** 114511.
59 S. Trost, K. Zilberberg, A. Behrendt, A. Polywka, P. Görrn, P. Reckers, J. Maibach, T. Mayer and T. Riedl, *Adv. Energy Mater.*, 2013, ***3,*** 1437–1444.
60 T. Leijtens, G. E. Eperon, S. Pathak, A. Abate, M. M. Lee and H. J. Snaith *Nat. Commun.*, 2013, 4, 2885.